Commensurability transitions in multilayers: A response to substrate-induced elastic stress

James M. Phillips and T. R. Story
Department of Physics, University of Missouri–Kansas City, Kansas City, Missouri 64110
(Received 13 April 1990)

Computer simulations of multilayers adsorbed on graphite show commensurability transitions between the two layers closest to the substrate. At low temperature, the first and second layers are mutually commensurate for films thinner than four layers. As the coverage is slightly increased to four layers, the three top layers form an expanded mutually commensurate slab that is incommensurate to the compressed first layer. As the temperature of the film is increased, the thermal expansion of the system drives the bottom layer into commensurability with the three-layer slab. These transitions appear to be caused by the elastic response of the film to the steep gradient in the substrate-adsorbate potential.

I. INTRODUCTION

Solid adsorbed films are elastic systems subject to nonuniform body forces originating out of the substrate. When these substrate-induced strains differ significantly from layer to layer, commensurability transitions may occur. In the course of our computer-simulation studies of adsorbed multilayers, structural transitions are observed as the film responds to increases in thickness and temperature. The purpose of this paper is to report these microscopic changes in the structure of the film as function of thermodynamically induced strains. The results are important because they improve our undersanding of new experiments[1,2] not explained by rigid structure models. In particular, the heat-capacity experiments of Zhu and Dash[1] show shifts in the melting temperatures of individual layers with increasing coverage. Our simulations confirm these shifts to be highly dependent upon the variation of the elastic stress in the film with height above the substrate.[3]

The role of elastic stress in the growth mechanisms of thin solid films has been anticipated by Dash[4] and by Nicholson and Parsonage.[5] Bruch[6] has derived a multilayer coexistence criterion that requires an increasing spreading pressure for layer-by-layer growth. Monson[7,8] has used computer simulation to study the compression of a film and observes wetting and prewetting transitions. Fluid interfaces have been reviewed by Rowlinson and Widom[9] and commensurate-incommensurate transitions by Bak.[10]

Controversies concerning the absolute thickness of the experimental films aside, the heat-capacity profiles of Zhu and Dash[1] clearly show an increase in relative coverage (and, consequently, more compression). Their unique pattern of layer-by-layer melting peaks demonstrates the role of compressive forces by observing the shift of individual layer melting temperatures in a direction and by an amount consistent with traditional thermodynamics and our simulations.

At present, the only computational tool sufficiently close to experiment to exhibit the microscopic detail of these properties is computer simulation. All computational methods have shortcomings when used to account for experiment—computer simulations are not an exception. The model and the method[11] used in this study have compared well with several experiments[1,2,12] and theoretical crosschecks.[6,13] An important consideration in testing simulations is to study a broad range of system parameters (temperature, density, system size, boundary conditions, ensemble type, and interaction potentials) to find the boundaries of reliability. The overall project is of such proportions that we have hopefully identified the relevant pitfalls. The results of the report are well within qualitative comparisons. Laboratory samples undergoing structural transitions are very sensitive to the system parameters. Our simulation results should be viewed as those of a model which scales approximately to a multilayer of argon, krypton, or xenon on graphite.

Recently, Hruska and Phillips[11] found a new mutually modulated structure for incommensurate layers within a solid film of methane adsorbed on graphite. In contrast, the layers of an argon bilayer were mutually commensurate. During our computational effort to simulate multilayer systems over a sizable region of the phase diagram, the structural transformations between three particular configurations (see points $A-C$ in Fig. 1) are especially interesting as an illustration of what can happen within films.

The basic issue of this report is the investigation of the structural response in a system subject to an external potential. The particular problem involves adsorbed multilayers from two to four layers which are elastically strained by the substrate holding potential. Figure 2 schematically illustrates a film with a height-dependent elastic shear.

In Sec. II we attempt to show, by use of simple models, that shearing stresses within solid films have a dependence on height above the substrate. In Sec. III we briefly describe the model and the simulation methods. In Sec. IV we present the simulation results for three regions of the phase diagram involved in commensurability transitions between layers in the film. In Sec. V we summarize the results and conclusions.

II. THERMODYNAMICS AND STATISTICAL MECHANICS OF STRESS

In order to demonstrate the change in the intermolecular pressure with height above the substrate, we offer a discussion from a formal summary by Steele.[8] We then extend the argument to anisotropic elastic crystals.[14]

Steele writes one component of the pressure tensor as

$$p_{zz}(\mathbf{r})=\rho^{(1)}(\mathbf{r})kT-\int_z^\infty \frac{\partial u_1(\mathbf{r}_1)}{\partial z_{12}}\rho^{(1)}(\mathbf{r}_1)dz_1-\int_A d\mathbf{r}_1\int_{-\infty}^{z} dz_2\int_z^\infty dz_1\frac{\partial u_2(\mathbf{r}_{12})}{\partial(\mathbf{r}_{12})}\rho^{(2)} . \tag{1}$$

The adsorption potential is u_1 and the intermolecular pair potential is u_2. The single-particle density is $\rho^{(1)}$ and the pair distribution is $\rho^{(2)}(\mathbf{r}_{12})$. The definition of the spreading pressure (ϕ) is extended to

$$\phi A=\int[p_T(z)-p_{zz}(\mathbf{r})]d\mathbf{r} .$$

The current status of this analysis is well reviewed by Rowlinson and Windom.[9] In particular, the arbitrariness of the $p_T(z)$ (transverse) component is explained.

The more important physical terms in Eq. (1) to our study is defined by Steele to be the "intermolecular pressure" in the perpendicular direction to the surface, $\mathcal{P}_{zz}(\mathbf{r})$ (p. 245 in Ref. 8). $\mathcal{P}_{zz}(\mathbf{r})$ is the first and last terms on the right-hand side of Eq. (1).

The condition of hydrostatic equilibrium further demonstrates the effects of the substrate potential on $\mathcal{P}_{zz}(\mathbf{r})$,

$$\frac{\partial\mathcal{P}_{zz}(z)}{\partial z}=-\rho^{(1)}(z)\frac{\partial u_1(z)}{\partial z} . \tag{2}$$

The term $p_{zz}(\mathbf{r})$ is z independent in the fluid and nearly zero. Equation (2) demonstrates the vertical variability and the range of the stress in the fluid film due to the adsorption potential. A realistic picture of these relationships is given by Finn and Monson[7] through a novel computer simulation.

The films in our simulations are solid multilayers. One should note that basic equilibrium thermodynamics can be generalized to crystal systems where anisotropic stresses and strains exist. Usually, elastic materials are studied under conditions of uniform applied stresses, resulting in uniform strains throughout the lattice. In a solid film, however, the stress and strain tensors vary with height above the substrate. The internal forces of the film may be thought of as anisotropic analog of the fluid problem discussed above. The elastic constants for the system, defined for a reference configuration, are also z dependent. Higher orders of approximation may be required to describe the configuration accurately.

In strict analogy to a pressure-volume system, a linear approximation to the work can be written

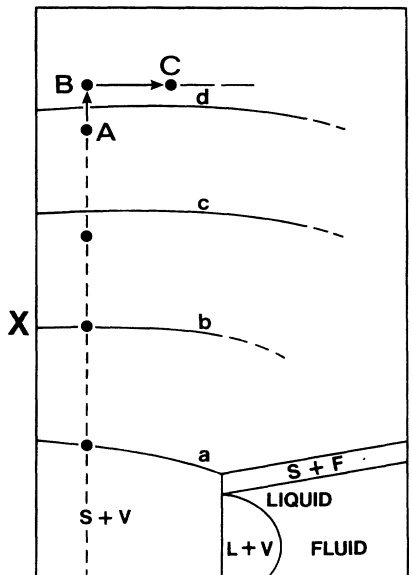

FIG. 1. Section of the multilayer phase diagram for coverage X, in monolayers, vs the temperature as a fraction of the bulk triple point, showing the positions of the principal points in the observed commensurability transitions. Between points A and B, layers 1 and 2 experience a C-IC transition. The simulation results for points B to C show the system reversing through an IC-C transition. The lower section of the figure shows the monolayer phases. Lines a, b, c, and d mark the completion of the solid monolayer, bilayer, trilayer and four-layer, respectively. The vertical dashed line is the $0.25T_t$ isotherm. The solid dots mark the coverages of 1.0, 2.0, 2.84, 3.87, and 4.2 ML. The temperature at point C is $0.40T_t$. The topmost layer is observed to disorder at $0.80T_t$.

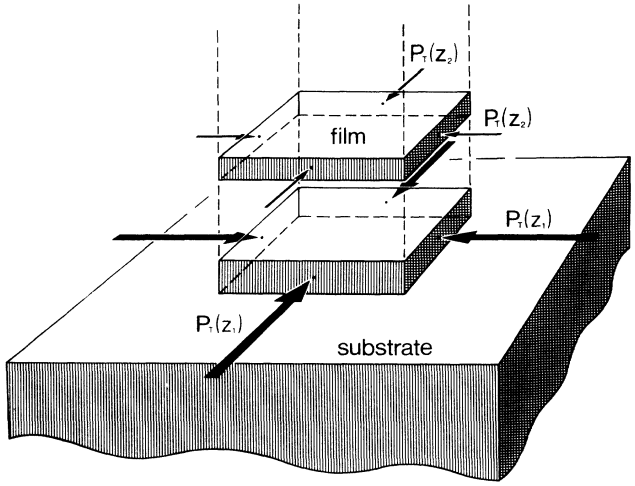

FIG. 2. Diagram showing the components of stress in an adsorbed film. The figure attempts to illustrate the height dependence of the shearing stress. The transverse components are depicted to be larger at z_1 than at z_2.

$$dW' = -\int_{\text{surface}} \sum_{i,j,k} (\tau_{ij}^{(0)} + \alpha\tau_{ij}^{(1)} + \cdots)\Delta u_{ik} X_k \, dS_j = -\int_{\text{volume}} \frac{\partial}{\partial x_j} \left[\sum_{i,j} (\tau_{ij}^{(0)} + \alpha\tau_{ij}^{(1)} + \cdots) \left[\sum_k \Delta u_{ik} \right] \right] dV \ . \tag{3}$$

In a uniformly stressed elastic solid, τ_{ij} and Δu_{ij} are constants; here they are not. Consequently, they remain a part of the integrand. The variables are defined as follows.

The work, dW', done by the lattice against the applied stresses in going from the configuration $\mathbf{R}$ to $\mathbf{R}+d\mathbf{R}$ is written in terms of the forces f_i on the area S_i of the ith face of the configuration R.[14] The ith component of the force action on the differential surface area dS is given by

$$f_i = \sum_j \tau_{ij} dS_j \ ,$$

where τ_{ij} represents the applied stress tensor. Without a net torque on the crystal, τ_{ij} is symmetric. Let Δu_{ij} be the displacement gradients of the strain $\Delta\mathbf{R}$. Then, it follows that the displacement of $d\mathbf{S}$ in the ith direction is

$$\Delta X_i = \sum_{j,k} \Delta u_{ij} X_k \ .$$

A linear approximation to the work done by the crystal against the applied stress to $d\mathbf{S}$ is written

$$-\sum_i f_i \Delta X_i = -\sum_{i,j,k} \tau_{ij} dS_j \Delta u_{ik} X_k \ .$$

The total work, dW', is obtained by integrating over the surface. The surface-to-volume integration is by Gauss's theorem. In Eq. (3) the presence of a body force requires τ_{ij} to be approximated. A first-order linear expansion is sufficient for this simple model analogy. We extend the discussion of Steele[8] and Wallace[14] to a spatially varying body force by letting

$$\tau_{ij} = \tau_{ij}^{(0)} + \alpha\tau_{ij}^{(1)} + \cdots \ ,$$

where α is an expansion parameter, $\tau_{ij}^{(0)}$ is the traditional stress applied to the film boundaries, and $\tau_{ij}^{(1)}$ is the nonuniform stress due to the z-dependent body forces, i.e., substrate potential. The term $\tau_{ij}^{(0)}$ contains the very small vertical compression applied to the top of the film by the vapor. The term $\tau_{ij}^{(1)}$ contains the compression due to the body forces (substrate potential). In an elastic continuum, orthogonal shearing stresses accompany the vertical component. It is our contention these shearing stresses cause the commensurate-incommensurate transitions seen in the simulations.

Consider another example of stress tensors for systems with body forces. Equation (2) states the equilibrium condition for a fluid. In an elastic system, the equations of equilibrium are a result of the Euler-Cauchy stress principle. Given an elastic system subject to a body force $\mathbf{F}$ per unit mass, the static state is described by

$$\frac{\partial \tau_{ij}}{\partial x} + F_j = 0, \quad i,j = 1,2,3 \ .$$

The body force is vertical ($j=3$). Therefore, $F_1 = F_2 = 0$ and

$$F_3 = -\frac{1}{m} \frac{\partial u_1(z)}{\partial z} \ .$$

Evaluating F_3 at z_1 and z_2, the heights of the first and second layers, respectively (see Fig. 3), clearly show a significant change in slope of the substrate potential. Between layers 1 and 2, there is usually a sign difference as well. The change is much less for higher comparisons. The difference in the value of

$$F_3(z_1) = -\left[\frac{\partial \tau_{xz}}{\partial x} + \frac{\partial \tau_{yz}}{\partial y} + \frac{\partial \tau_{zz}}{\partial z} \right]_{z_1}$$

at z_1 compared to the value at z_2 indicates a stress gradient between the layers. There must be an accompanying shear. The x and y gradients are zero over a given plane. Equation (2) compares the vertical density $N(z)$ to the film stress. Figure 3 gives a phenomenological picture of the extent of the stress with height above the substrate.

The shear components in the x-y plane (parallel to the substrate) resulting from the compression in the vertical direction will correspondingly differ significantly from

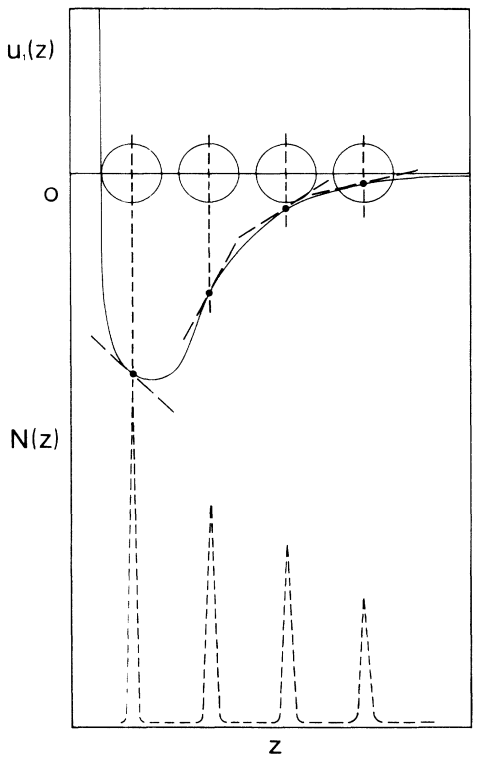

FIG. 3. Schematic drawing showing the slope of the adsorption potential $u_1(z)$ and the vertical density $N(z)$ for a film. These plots and the relationships for F_3 given in the text demonstrate that the body forces in the film clearly depend upon z.

layer 1 to layer 2. When this difference exceeds a threshold, the first and second layers become mutually incommensurate. The simulation results that follow show coverage- and temperature-driven examples of such a transition.

The purpose of the simulations is to observe the structural response of the multilayer to the substrate-imposed stresses analogous to the transverse terms of Eq. (1). Through structural distribution functions and ensemble-averaged structure factors, the simulations present evidence of the response of the crystal to the difference in the transverse components as one moves from the height of layer 1 to the height of layer 2.

III. THE MODEL AND THE SIMULATION METHODS

The canonical-ensemble (NVT) simulation details were described previously.[11] Our Monte Carlo algorithm uses a Lennard-Jones (LJ) pair potential (reduced variables for corresponding states scaling) for the adsorbate atoms and the $\Sigma(10,4)$ adsorption potential by Steele.[15] The system consists of 672 particles in a rectangular box with a vertical dimension of 20 molecular diameters and periodic boundary conditions in x and y only. We assume the graphite substrate to be smooth. This allows corresponding-states scaling. Since experiments show argon to be incommensurate to the graphite at our temperatures and coverages, the loss to realism is slight. Parallel studies of systems with different substrates have shown the simulations to be sensitive to system dependent effects, i.e., layer-to-layer commensurability. The results reported in this paper are a small fraction of those generated. The simulations have been started from many different configurations. When a computationally equilibrated system has the same results as one achieved by an entirely different quasistatic path, the uniqueness of those results is quite reasonable. Series of runs along isotherms are confirmed by other series along intersecting isochores. Artificial effects due to simulation abnormalities are well identified and reported in the results below.

During each simulation ($>20\,000$ moves per particle) the ensemble averages are taken for the internal energy, the three-dimensional (3D) virial, the 2D pair distribution for all individual layers, and the vertical probability distribution function. A careful examination of the evolution of these averages ensures computational stability. The structure of the film is given by the ensemble averages for two distribution functions. The vertical density distribution $N(z)$ is the probability of finding a molecule in the range z to $z+dz$ above the substrate. The structure within a layer is given by a 2D pair distribution function $G(R)$. The pair distribution is defined to give the number of atoms, dn, in a circular ring of radius R and thickness dR to be

$$dn = 2\pi R n_0 G(R)\,dR \ ,$$

where n_0 is the 2D number density of the individual layer. As explained in an earlier paper,[11] the normalization of $G(R)$ is only approximate. An additional tool has been added to these simulations, namely the two-dimensional structure factors $S(\mathbf{k})_n$ of individual layers. In keeping with our previous work,[16] a 2D fictitious structure factor $S(\mathbf{k})_n$ (layer order parameter[17]) is given for the N_n atoms in the nth layer. Well after equilibration, the simulation is restarted, and an additional ensemble average is taken for

$$S(\mathbf{k})_n = \left\langle \left| \sum_{i<j}^{N_l} e^{i\mathbf{k}\cdot\mathbf{r}_{ij}} \right|^2 \right\rangle \Big/ N_n \ .$$

N_n is monitored for particle exchanges during the averaging. The vector $\mathbf{r}_{ij}$ is the spatial position of the atom pairs in the layer. The vector $\mathbf{k}$ taken to be a large array centered on a reciprocal-lattice vector $\mathbf{G}_n$. For $\mathbf{k}$ equal to $\mathbf{G}$, the layer Debye-Waller factor $2M_n$ is given by

$$2M_n = -\ln[S(\mathbf{G})/N_n] \ .$$

Slight rotations and drifts of the simulation cell are accounted for in the averaging. In addition, the ensemble averaging of $S(\mathbf{k})_n$ allows us to identify effects by the boundary conditions on the structure. In the results reported below, we used six $\mathbf{G}_i$ vectors and 17×17 arrays in reciprocal space. As a consequence, these simulations are critically monitored. Any departure of a layer from a strict 2D triangular lattice is noted in the accurate $G(r)$ and is very pronounced in the $S(\mathbf{k})_n$. The simulation cell is exact for 224 particles, and is, therefore, not quite square. The symmetrical response of the layers with $N_n \neq 224$ is a precise measure of the extent to which the periodic boundary conditions influence the layer structure.

There is some confusion in the literature about isobaric ensembles, etc., and the strict NVT ensemble used in these simulations. In studying fluid films, Finn and Monson[7] show the advantages of simulating film growth at a fluid-vapor boundary by a realistic and clever method. Our simulations use a fixed ceiling of the simulation box, whereas Finn and Monson adjust the height of the ceiling during the isobaric simulation to keep the 3D gas pressure constant. In the simulations reported here, the system is solid and the vapor phase is so dilute that any attempt to control the 3D gas pressure is not wise.

Krim[18] reports that the ratio of the cohesive energy of the adsorbates to the C_3 coefficient in the adsorption potentials is nearly the same for systems of argon-graphite, krypton-graphite, and xenon-graphite. Thus, by corresponding-state scaling, the simulations would apply equally to all three systems. The ratio of the attractive well depth of the atoms in the film to the atom-substrate interaction is 6.95. The potential minimum for the LJ(12,6) interactions are taken to be 143.2 K/ϵ for argon, 190 K/ϵ for krypton, and 230 K/ϵ for xenon. We have scaled all temperatures to the system 3D triple-point temperature T_t. Hansen and Verlet[19] found the triple-point temperature of a LJ(12,6) system to be $T_t = 0.7\epsilon$. This value has been confirmed for these simulations.

Experiments will differ from these simple model results for several reasons. We have studied this issue very carefully in the past. The repulsive part of these interaction potentials is slightly soft[20] and the substrate-mediated effects[21] are missing. The argon system will have zero-

point effects to a greater degree than the others. The quantitative differences have been precisely described by Bruch[22] and by Phillips and co-workers.[23] Unless one is willing to include *all* of the subtle realistic effects, improvements on the simple models used here are probably fortuitous.

IV. SIMULATION RESULTS

The results of the simulations presented in this section are principally structural. However, thermodynamic properties and their fluctuations were monitored throughout each simulation in order to ensure computational equilibration. The structures of the simulated films are given in terms of the adsorbate 2D pair distributions $G(R)$ for each layer, the vertical distribution $N(z)$, overhead "snapshots" of atom positions, and structure factors of individual layers. It is our intent that this structural information will account for the diffraction studies of the past[1] as well as for proposed new experiments.

This section is organized to give the results taken at points $A-C$ in Fig. 1. Table I lists the location, maxima, and width at half maximum (WHM) of the peaks in all $N(z)$ reported. Before giving those results, we report on two lower coverages on the $0.25T_t$ isotherm. First, the reference structure of a complete bilayer is given for temperature $T=0.25T_t$ and coverage $X=2.0$ ML (ML denotes monolayer). The close comparison of the simulation with experiment[1] demonstrates the ability of the system to mirror correct structure with minimal computational artifacts.

The units of coverage are given in uncompressed monolayers at low temperature. A series of test simulations were done to determine the coverage $X=1.0$ ML for a monolayer with a two-dimensional virial (spreading pressure) equal to zero. Figure 4 is a plot of both $G(R)$ for layers 1 and 2 superimposed. There are 100 points between each unit of σ averaged over 20 000 Monte Carlo moves per particle and 224 particles per layer. The single-layer lattices are perfect triangular structures that form an AB mutually commensurate bilayer. Figure 4(b) is the averaged vertical density $N(z)$ for the same simulation.

The results are presented for an argon-graphite scaling, but they are usable for krypton or xenon on graphite with corresponding states. Figure 5 shows the first and second layers to be still mutually commensurate at the same temperature, but with the coverage increased to $X=2.84$ ML.

TABLE I. Values of the vertical density $N(z)$ for the peak positions, the maximum, and the width at half maximum (WHM). The temperatures and coverages are given in the units defined in the text.

$\frac{T}{T_t}$	X (ML)	$\frac{z_{max}}{\sigma}$	$N(z_{max})$	WHM
0.25	2.00	0.88	10.0623	0.0466
0.25	2.00	1.78	5.0478	0.0921
0.25	2.84	0.87	8.3181	0.0421
0.25	2.84	1.76	4.3761	0.0764
0.25	2.84	2.67	2.5819	0.0825
0.25	3.87	0.88	5.6646	0.0459
0.25	3.87	1.78	3.4469	0.0753
0.25	3.87	2.69	2.6395	0.0899
0.25	3.87	3.59	1.5274	0.1119
0.25	4.20	0.88	5.2153	0.0466
0.25	4.20	1.79	3.4118	0.0690
0.25	4.20	2.69	2.8483	0.0821
0.25	4.20	3.59	1.9624	0.1089
0.25	4.20	4.49	0.0627	0.1222
0.40	4.20	0.88	4.1078	0.0584
0.40	4.20	1.79	2.4208	0.0950
0.40	4.20	2.69	1.7956	0.1216
0.40	4.20	3.61	1.1448	0.1534
0.40	4.20	4.47	0.1551	0.2458

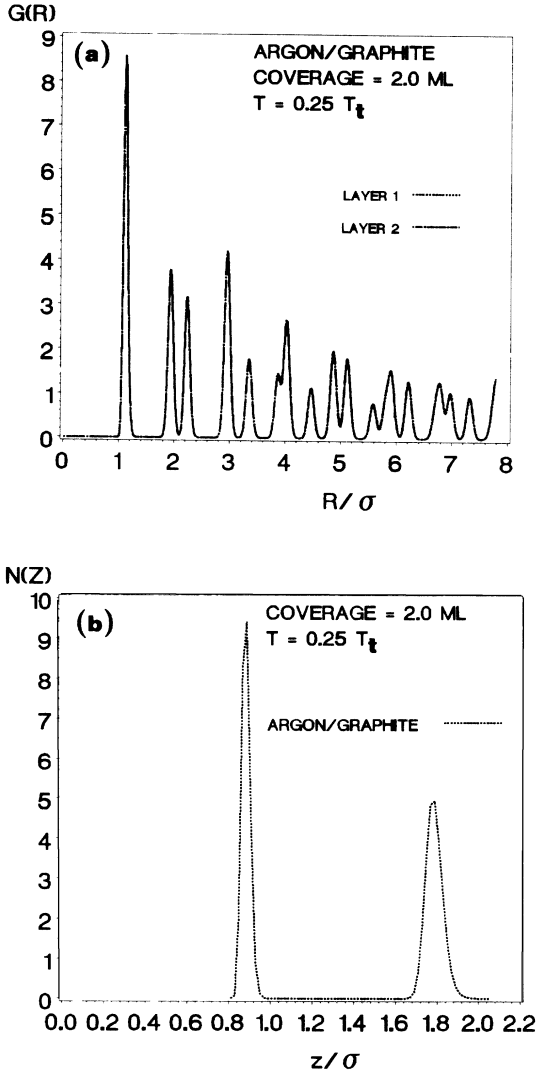

FIG. 4. (a) Plot of the 2D pair distributions for both layers of an argon-graphite bilayer. These mutually commensurate layers have their distributions superimposed. (b) Plot of the vertical density for the same simulation. The peaks are not modulated, and their positions are precisely those of a triangular lattice.

A. Results for point *A*

The mutually commensurate structure between layers 1 and 2 on this isotherm ($T=0.2T_t$) continues upward for coverages including 3.87 ML (Fig. 6). The population of layer 1 is 187 particles. There are two vacancies in layer 2; note that the region around the vacancies is not elastically distorted into a pair of edge defects (Fig. 7). This condition changes at higher temperature. Close inspection of the pair distributions for high-order peaks (Fig. 6) shows a very slight asymmetry in the aspect ratio for the mutually commensurate layers 1 and 2. In spite of this, the effects of the boundary conditions are barely detectable. This slight effect in real space is more visible in the $S(\mathbf{k})_n$, of course. The point is that periodic boundary effects are present at some points in our project. They are very small, and extensive testing in real and reciprocal space suggests they are not the driving force of the commensurability transitions. By comparing the results for both perfect and intentionally altered models, subtleties in the structure factors indicate when and to what extent artificial simulation effects enter the results.

B. Results for point *B*

The coverage is increased to just over four layers, $X=4.2$ ML, while the temperature is held to the $0.25T_t$ isotherm. This structure is quite important because there has been a commensurate-incommensurate (C-IC) structural transition between layers 1 and 2 as the system moved from point *A* to *B* in Fig. 1. The solid film has reponded to the increasing shear between these two layers

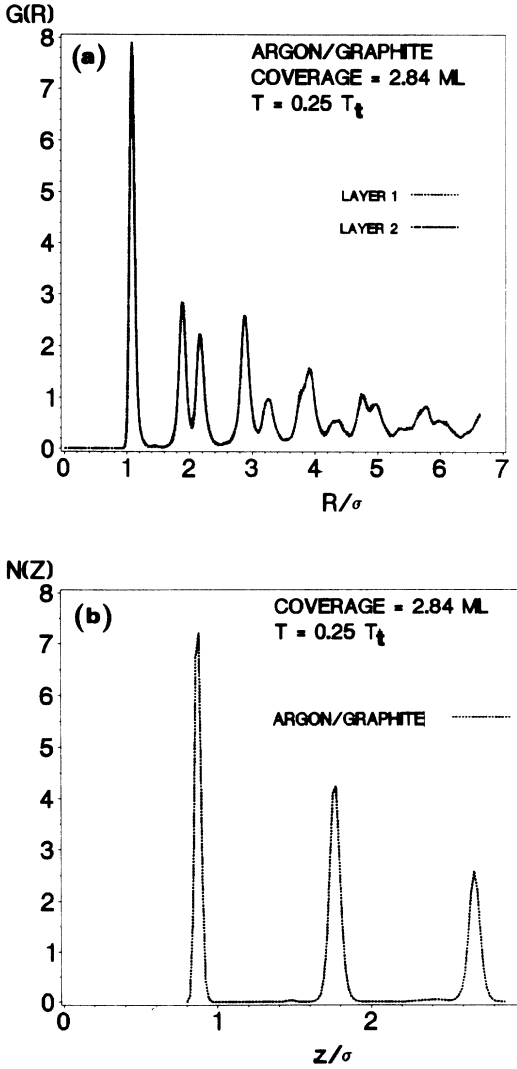

FIG. 5 (a) Plot of the 2D pair distributions for layers 1 and 2 of an argon-graphite multilayer. These mutually commensurate layers have their distributions superimposed. (b) Plot of the vertical density for the same simulation.

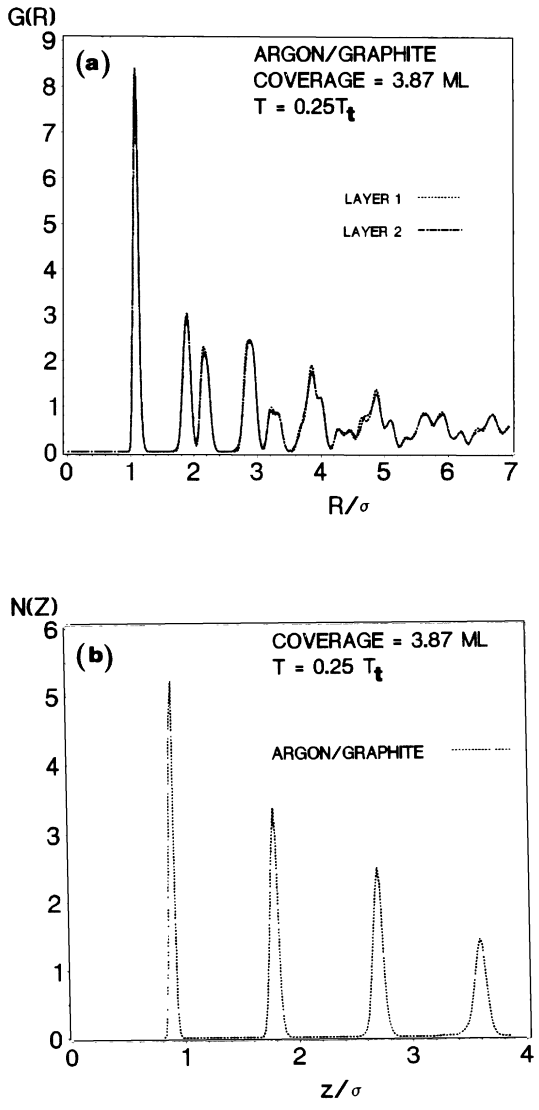

FIG. 6. (a) Plot of the 2D pair distributions for layers 1 and 2 of an argon-graphite multilayer. These mutually commensurate layers have their distributions superimposed. (b) Plot of the vertical density for the same simulation. The results were taken at point *A* of Fig. 1.

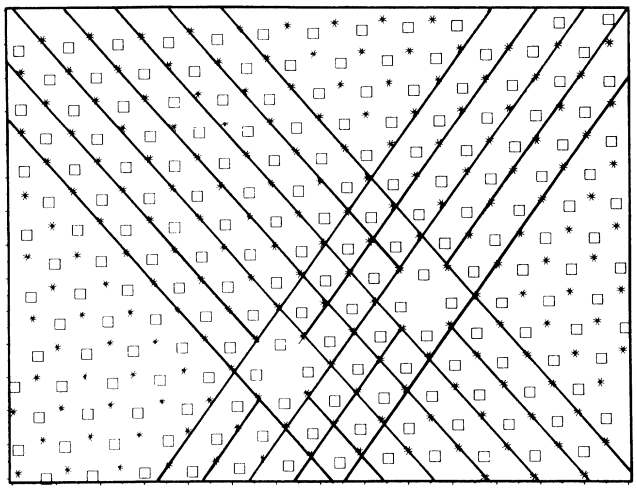

FIG. 7. Overhead view of the atom positions of layer 1 (□) and layer 2 (*) only. The configuration is from point A ($X=3.87$ ML and $T=0.25T_t$). There are two vacancies in layer 2. The added lines emphasize the lack of elastic distortion in the neighbor of the vacancies.

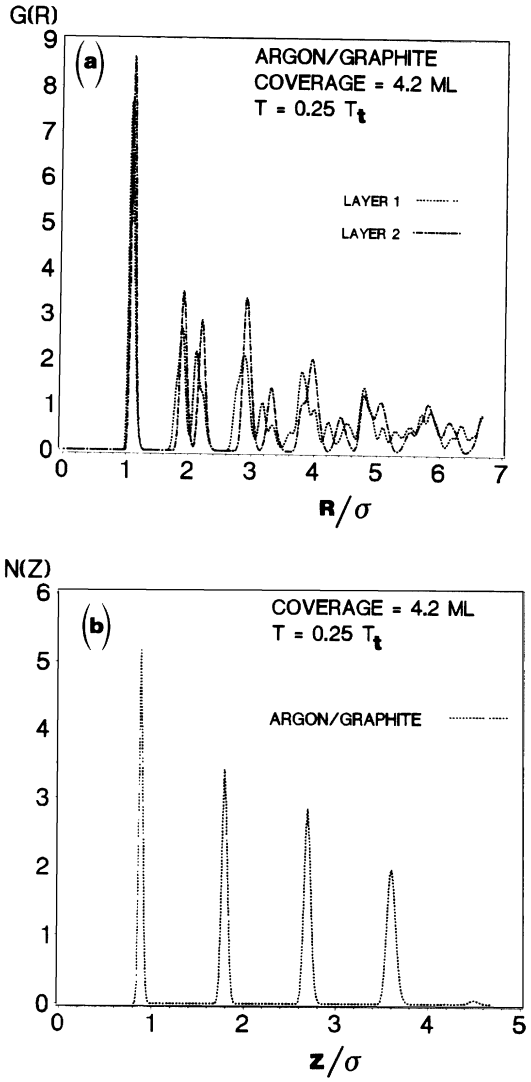

FIG. 8 (a) Plot of the 2D pair distributions for layers 1 and 2 of an argon-graphite multilayer. The layers are clearly incommensurate. (b) Plot of the vertical density for the same simulation. The results were taken at point B of Fig. 1.

(Fig. 3). The elastic threshold has been exceeded and the lattice constants now differ between the two layers (Fig. 8). The top of the film is now a mutually commensurate three-layer ABC slab (Fig. 9). The slab structure is three layers of fcc crystal in the [111] direction. Stripping away all other atoms, the $S(\mathbf{k})_n$ for these three commensurate layers individually gives perfect triangular lattices to better than 0.1% in the length and angle of the lattice vectors of that layer. It is important to note that the effects of the periodic boundary conditions are undetectable. This three-layer section is now available as the epitaxial template for future growth. Further increases in coverage will result in structures not strongly influenced by the layer closest to the substrate, whereas, for coverages below four layers, each additional layer—upon completion—is compressed to commensurability with the lattice matching the lowest layer. The threshold for the C-IC transition appears to need not only a sufficient shearing stress between the successive layers, but also the existence of at least three layers of compressed bulklike structure for a rigid growth template. This is a contrast to CH_4/graphite,[11,13] where the simulated bilayer is mutually incommensurate and the trilayer relaxes from overcompression relative to the bulk.[1]

Layer modulation between incommensurate systems is an active area of study.[24–26,10] In the CH_4/graphite bilayer, we found the layers to modulate each other mutually to form a pair of oblique triangular lattices. Both layers have relatively soft elastic constants. In this case, however, the system is more like the Novaco-McTague[24] system. Here, however, the rigid lattice acts from *above*. Layer 1 has an oblique 2D unit cell (Fig. 10). The second and higher layers are not detectably altered from strict triangular lattices. The structure of layer 1 is similar to that found in the CH_4/graphite system,[11] except that the difference in the magnitude of the lattice constants is considerably less. In Fig. 8 the splitting of the peaks in $G(R)$ is only noticeable in the higher-order neighbors. In methane the first-neighbor peak was clearly divided. The stronger holding potential would account for this difference. Figure 10 shows the three different interfacial accomodations present at the same structure. One set of rows is essentially commensurate, i.e., those rows parallel to the $\mathbf{b}_1$ lattice vector. Those rows parallel to the $\mathbf{a}_1$ lattice vector are rotated from the layer-2 direction. The rows in the $\mathbf{b}_1$-$\mathbf{a}_1$ direction form a domain-wall structure. The choice of directions in the simulation is quite random. We believe it infers that the structure in Fig. 10 is just a small window of the type of structure previously observed in krypton monolayers on graphite showing large hexagonal domain networks. The angle of rotation is quite close to that predicted by simple Novaco-

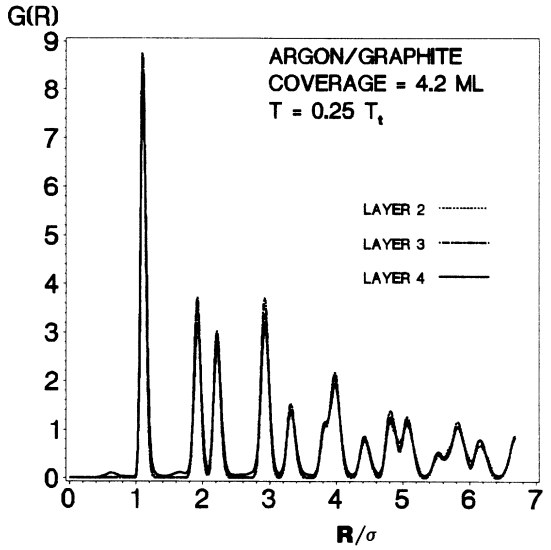

FIG. 9. Plot of the 2D pair distributions for layers 2, 3, and 4 for the simulation at point B of Fig. 1. These three layers are mutually commensurate and they are incommensurate to the compressed layer 1 (Fig. 8). The peaks are modulated and their positions are precisely those of a triangular lattice.

McTague theory. The magnitudes for domain-wall thickness and the rotations are surely affected by the small size of our sample cell. The topology of the structure is quite consistent with the krypton-graphite system.[26] (See Ref. 11 for a more extended discussion of this unusual structure.) Bruch[22] has recently performed a perturbation-theoretic calculation on a similar system and found the incommensurate structure to be a rectangular centered lattice. What we have called an oblique lattice is, in fact, close to the Bruch prediction, the difference being primarily the angle between the lattice vectors, 85° in the simulation to 90° in the perturbation calculation. In the simulation the results from the structure-factor calculation shows that one angle is locked at 60°. The reason for the difference could be a combination of effects. The simulation may be influenced by the boundary conditions, or the calculation could be lacking sufficient thermal disorder. Since the structure factor for the single incommensurate layer shows a small asymmetry due to the boundaries, the simulation of a very large system may move toward the calculated structure.

C. Results for point C

Another transition is observed when the temperature increases to $T=0.40T_t$ while keeping the coverage con-

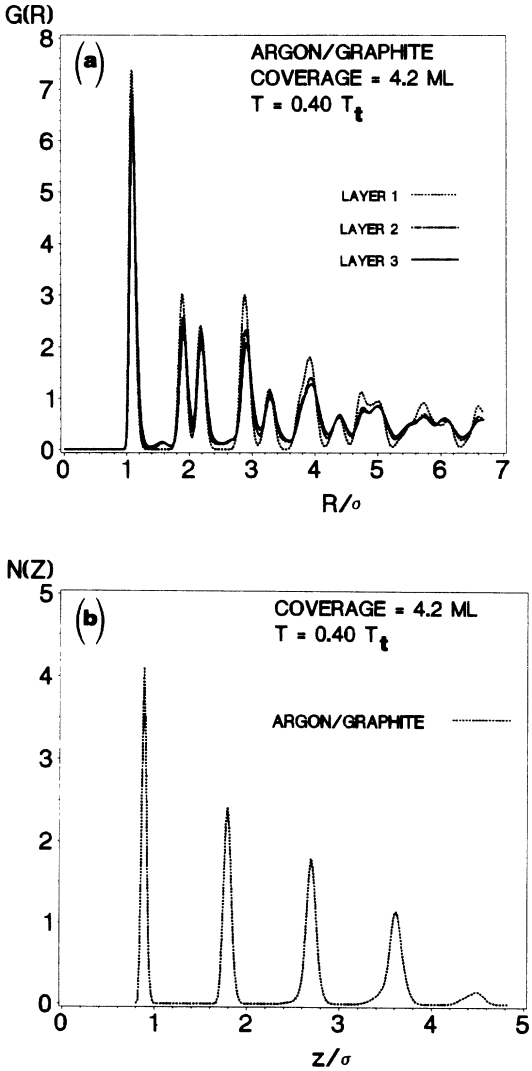

FIG. 11. (a) Plot of the 2D pair distributions for layers 1 and 2 of an argon-graphite multilayer. These mutually commensurate layers have their distributions nearly superimposed. (b) Plot of the vertical density for the same simulation. The results were taken at point C of Fig. 1.

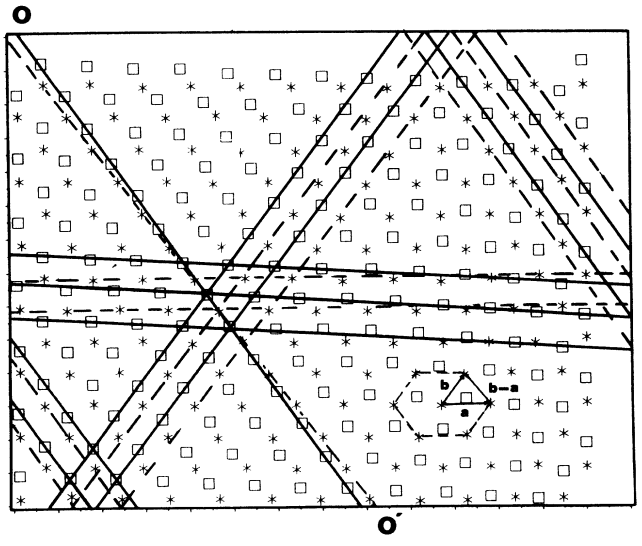

FIG. 10. Overhead view of the atom positions of layer 1 (□) and layer two (*) only. The configuration is from point B ($X=4.2$ ML and $T=0.25T_t$). This diagram illustrates the modulation of layer 1 from above by the relatively rigid three-layer slab shown in Fig. 9.

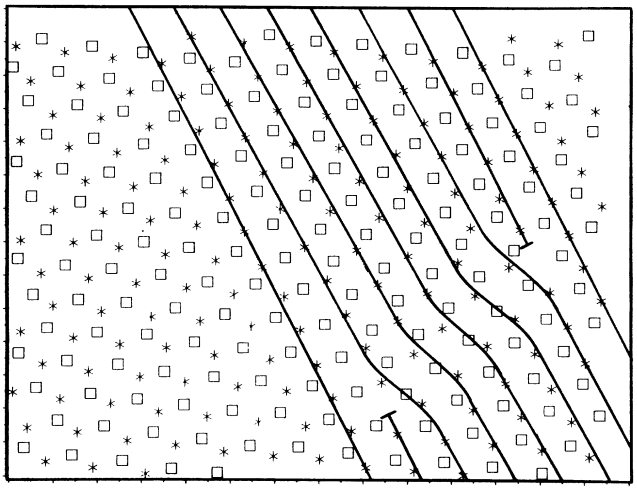

FIG. 12. Overhead view of the atom positions of layer 1 (□) and layer 2 (*) only. The configuration is from point B ($X=4.2$ ML and $T=0.40T_t$). There is a pair of edge dislocations in layer 2. The added lines emphasize the elastic distortion in the neighbor of the vacancies. This is in contrast to Fig. 7.

stant, $X=4.2$ ML. The additional thermal energy has expanded layer 1 to the point where it returns to commensurability with the already mutually commensurate layers 2 and 3 (see Fig. 11). Hence, a temperature-driven IC-C structural transition has occurred between layers 1 and 2. From points B to C, the density of the first layer has dropped 1.7%; that for layer 2, 1.1%.

Layer 2 has an edge-defect pair. This is in contrast to point A, where the defects were merely vacancies. The periodic potential of the commensurate templates above and below layer 2 was sufficiently strong that the elastic distortion in the vacancy neighborhood was not thermally activated (point A). At point C (see Fig. 12) the rows of atoms in layer 2 are elastically strained to form the classic defect pair.[27]

When the temperature is increased further on the $X=4.2$ ML isochore, the system reverts to the IC structure observed at point B. Layer 4 increasingly disorders as the temperature approaches $T=0.8T_t$[3].

V. SUMMARY AND CONCLUSIONS

In an extensive series of computer simulations of multilayer films, a C-IC transition is observed in the mutually registered structure of the first and second layers closest to a graphite substrate. This transition occurs along the $T=0.25T_t$ isotherm as the coverage increases from just below four complete layers to just above them. A second transition follows when the coverage is held at 4.2 ML and the temperature is increased to $0.40T_t$. The film returned to a mutually commensurate structure between the first and second layers. These transitions are unique in that they provide physical examples of stress- and temperature-driven commensurability transitions discussed by Gordon and Villain[28] in a formal context.

The formation of a mutually commensurate three-layer section above a compressed first layer provides important insight into the possibility of a shift in periodic templates controlling the epitaxial growth of very thin solid films. For systems with argon-graphite scaling (also krypton or xenon on graphite), the periodicity pattern governing solid-on-solid growth changes from the highly compressed layer closest to the substrate to the mutually commensurate slab on the vapor side of the adsorbate. Although the particular coverage marking the template change in this simulation model is ~4, experimental studies may differ from this elementary characterization. The qualitative evidence given by this simulation result is so clear, however, that it strongly suggests the possibility of such transitions in real films.

The range of application the simulation model may be narrow because the CH_4/graphite system, with its relatively stronger holding potential, is not mutually commensurate in the first two layers at any coverage. Substrate-mediated effects and quantum contributions (argon) will alter the application of corresponding states. The simulations indicate a strong possibility that systems which scale close to this model may undergo commensurability transitions between the first and second layers. The existence of these structures would have important implications in regard to the laboratory results, in ways not yet fully understood. The realization of the possibility of such structures should be helpful in further examining experimental data.

A phenomenological presentation of the existence of shearing stress between layers close to the substrate was given in Sec. II. Although these arguments form an imprecise description at the atomic level, the response of the physical system demonstrated in the simulations is quite compelling.

ACKNOWLEDGMENTS

One of us (J.M.P.) would like to thank W. A. Steele, J. Z. Larese, L. Passell, P. A. Monson, L. W. Bruch, and H. Taub for many helpful discussions in the development of this project. He would also like to thank J. G. Dash for his hospitality, his advice, and his strain data prior to publication.

[1]J. Z. Larese, M. Harada, L. Passell, J. Krim, and S. Satija, Phys. Rev. B **37**, 4735 (1988); J. Z. Larese and Q. M. Zhang, Phys. Rev. Lett. **64**, 922 (1990); J. Z. Larese, Q. M. Zhang, L. Passell, J. M. Hastings, J. R. Dennison, and H. Taub, Phys. Rev. B **40**, 4271 (1989).

[2]Da-Ming Zhu and J. G. Dash, Phys. Rev. Lett. **57**, 2959 (1986); **60**, 432 (1988).

[3]James M. Phillips, Phys. Lett. A **147**, 54 (1990).

[4]J. G. Dash, *Films on Solid Surfaces* (Academic, New York, 1975), pp. 70 and 81, private communication.

[5]D. Nicholson and N. G. Parsonage, *Computer Simulation and the Statistical Mechanics of Adsorption* (Academic, London, 1982).

[6]L. W. Bruch and M. S. Wei, Surf. Sci. **100**, 481 (1980; M. S. Wei and L. W. Bruch, J. Chem. Phys. **75**, 4130 (1981); L. W. Bruch and X.-Z. Ni, Trans. Faraday. Soc. Discuss. **80**, 217 (1985); L. W. Bruch, J. M. Phillips, and X.-Z. Ni, Surf. Sci. **136**, 361 (1984).

[7]J. E. Finn and P. A. Monson; Mol. Phys. **65**, 1345 (1988); Phys. Rev. A **39**, 6402 (1989).

[8]W. A. Steele, *The Interaction of Gases with Solid Surfaces* (Pergamon, Oxford, 1974).

[9]J. S. Rowlinson and B. Widom, *Molecular Theory of Capillarity* (Clarendon, Oxford, 1982); P. Schofield and J. R. Henderson, Proc. R. Soc. London Ser. A **379**, 231 (1982); R. Evans, Adv. Phys. **28**, 143 (1979).

[10]P. Bak, Rep. Prog. Phys. **45**, 587 (1982).

[11]C. D. Hruska and James M. Phillips, Phys. Rev. B **37**, 3801 (1988); James M. Phillips and C. D. Hruska, *ibid.* **39**, 5425 (1989); James M. Phillips, Langmuir **5**, 571 (1989).

[12]J. J. Hamilton and D. L. Goodstein, Phys. Rev. B **28**, 3838 (1983); M. S. Pettersen, M. J. Lysek, and D. L. Goodstein, Surf. Sci. **175**, 141 (1986).

[13]James M. Phillips, Phys. Rev. B **34**, 2823 (1986) (paper III); **29**, 4821 (1984); **29**, 5865 (1984) (paper II); James M. Phillips and M. D. Hammerbacher, *ibid.* **29**, 5859 (1984) (paper I).

[14]D. C. Wallace, *Thermodynamics of Crystals* (Wiley, New York, 1970); Y. C. Fung, *Foundations of Solid Mechanics* (Prentice-Hall, Englewood Cliffs, NJ, 1965).

[15]W. A. Steele, J. Phys. Chem. **82**, 617 (1978).

[16]J. M. Phillips, L. W. Bruch, and R. D. Murphy, J. Chem. Phys. **75**, 5097 (1981).

[17]J. F. Lutsko, D. Wolfe, S. R. Philpost, and S. Yip, Phys. Rev. B **40**, 2841 (1989).

[18]J. Krim, Ph.D. thesis, University of Washington, 1984 (unpublished).

[19]J. P. Hansen and L. Verlet, Phys. Rev. **184**, 151 (1969).

[20]J. A. Barker, in *Rare Gas Solids,* edited by M. L. Klein and J. A. Venables (Academic, New York, 1976), Vol. I.

[21]L. W. Bruch, Surf. Sci. **125**, 194 (1983).

[22]L. W. Bruch, Trans. Faraday Soc. Discuss. **80**, 217 (1985), and private communication.

[23]James M. Phillips and L. W. Bruch, J. Chem. Phys. **83**, 3660 (1985); K. A. Hunzicker and James M. Phillips, Phys. Rev. B **34** (1986).

[24]A. D. Novaco and J. P. McTague, Phys. Rev. Lett. **38**, 1286 (1977).

[25]J. Villain, Phys. Rev. Lett. **41**, 36 (1978).

[26]H. Shiba, J. Phys. Soc. Jpn. **46**, 1852 (1979); **48**, 211 (1980).

[27]B. I. Halperin and D. R. Nelson, Phys. Rev. Lett. **41**, 121 (1978).

[28]M. B. Gordon and J. Villain, J. Phys. C **18**, 3919 (1985); M. B. Gordon and F. Laçon, *ibid.* **18**, 3929 (1985).